ACKNOWLEDGEMENTS

I would like to express my gratitude to all those who gave me the possibility to complete this thesis. I want to thank the School of Materials and Mineral Resources Engineering (SMMRE, Universiti Sains Malaysia) for giving me permission to commence this project and to do the necessary research work. I would like to extend my heartfelt gratitude to my supervisor Dr. Pung Swee Yong for his encouragement, guidance, support, patience and understanding during the research and writing of this dissertation. I also like to thank my Co-supervisor, Assoc. Prof. Dr. Zainovia Lockman for all of her advice and support.

I would like to thank the excellent technicians and administration staffs especially from School of Materials and Mineral Resources Engineering who have helped and assisted me in the characterization of lots of samples. I would like to thank them for their contributions and time.

My special thanks to husband, parents and friends that are always giving me support throughout in completing this dissertation. Last but not least, I would like to extend my gratitude to everyone whom may have contributed in one way or another to make this thesis a reality. Thank you very much.

May Allah SWT bless all of you.

TABLE OF CONTENTS

LIST OF TABLES

LIST OF FIGURES

LIST OF ABREVIATIONS

AA-CVD	Aerosol Assisted - Chemical Vapor Deposition
a.u.	Arbitary Unit
Ar	Argon
CVD	Chemical Vapor Deposition
EDX	Energy Dispersive X-ray
FE-SEM	Field Emission Scanning Electron Microscopy
HRTEM	High Resolution Transmission Electron Microscopy
$FeCl_3$	Iron Chloride
$Fe\ (NO_3)_3.9H_2O$	Iron Nitrate Nonahydrate
NRs	Nanorods
O_2	Oxygen
PL	Photoluminescence
RhB	Rhodamine-B
SEM	Scanning Electron Microscopy
Si	Silicon
TEM	Transmission Electron Microscopy
XRD	X-ray Diffraction Spectroscop
XPS	X-Ray Spectroscopy
Zn	Zinc
ZnO	Zinc Oxide

LIST OF SYMBOLS

cm	Centimetre
°	Degree
Θ	Degree
°C	Degree Celsius
°C/min	Degree Celsius per minute
g	Gram
keV	Kiloelectron-Volt
<	Less than
M	Meter
µm	Micrometer
mL	Millilitre
min	Minute
M	Mole
>	More than
nm	Nanometer
Nm	Nanometer
Ω	Ohm
%	Percentage
±	Plus minus
S	Second
sccm	Standard Cubic Centimeter
T	Temperature
Λ	Wave length

LIST OF PUBLICATIONS

International peer-reviewed journal

1. Abd Aziz, S. N. Q. A, Pung, S. Y., & Lockman, Z. (2014). "Growth of Fe-doped ZnO nanorods using Aerosol Assisted-Chemical Vapour Deposition via *in-situ* doping" *Applied Physics A* 116 (2014) 1801-1811(ISI cited, impact factor: 1.545).

2. Abd Aziz, S. N. Q. A, Pung, S. Y., Lockman, Z. & Hamzah, N. A. (2014). "Structural and optical properties of Fe-doped ZnO nanorods" *Adv. Mater. Res.* 854 (2014) 151-158 (ISI cited).

3. Abd Aziz, S. N. Q. A**.,** Pung, S.-Y., Ramli, N. N. & Lockman, Z. (2014). "Growth of ZnO nanorods on stainless steel wire using chemical vapour deposition and theirs photocatalytic activity" *The Scientific World Journal* (2014) doi:10.1155/2014/252851 (ISI cited, impact factor: 1.730).

4. Abd Aziz, S. N. Q. A**,** Pung, S. Y., Lockman, Z., Hamzah, N. A. & Chan, Y. L. "*Ex-situ* doping of ZnO nanorods by spray pyrolysis technique" *Mater. Sci. Forum* 756 (2013) 16-23. (ISI cited).

International conference proceedings

1. Abd Aziz, S. N. Q. A, Pung, S. Y., & Lockman, Z. "Growth of Fe-doped ZnO nanorods using aerosol assisted-chemical vapour deposition via *in-situ* doping". Mini Symposium USM-NUT (Nagaoka University Technology), Universiti Sains Malaysia, Penang, Malaysia (21-22 Oct. 2013).

2. Abd Aziz, S. N. Q. A, Pung, S. Y., Lockman, Z., Hamzah, N. A. & Chan, Y. L. "Structural and optical properties of Fe-doped ZnO nanorods", Proceeding of the 5th Regional Conference on Materials Engineering and the 5th Regional Conference on Natural Resources and Materials 2013 (RCM5 & RCNRM5) (21-23 Jan 2013).

3. Abd Aziz, S. N. Q. A, Pung, S. Y., Lockman, Z., Hamzah, N. A. & Chan, Y. L. "*Ex-situ* doping of ZnO nanorods using spray pyrolysis technique", The 3rd ISESCO International Workshop and Conference on Nanotechnology (IWCN 2012), Kuala Lumpur, Malaysia (5-7 Dec 2012).

SINTESIS DAN PENCIRIAN Fe-DOP ROD ZINK OKSIDA

ABSTRAK

Teknik Pemendapan Wap Kimia (CVD) adalah salah satu pengedapan wap yang paling biasa digunakan oleh penyelidik untuk mensistesis ZnO berstruktur nano. Walau bagaimanapun, pendedahan semasa mengenai cara pendopan *in-situ* dengan menggunakan CVD tidak memberi banyak fleksibiliti bagi penyelidik untuk menghasilkan ZnO terdop berstruktur nano. Dengan itu larutan bahan dop ditempatkan di luar relau, teknik Aerosol Pembantu Pemendapan Wap Kimia (AA-CVD) berpotensi sebagai teknik pendopan *in-situ* kerana menawarkan banyak kelebihan seperti fleksibiliti mengawal kepekatan larutan bahan dop, tempoh pendopan, jenis pelopor pendopan dan berpotensi dalam pengeluaran ZnO terdop berstruktur nano secara besar-besaran. Projek ini bermula dengan membangunkan sistem CVD untuk menghasilkan ZnO bersaiz nanometer tanpa dop dengan tidak menggunakan pemangkin asing. Kajian sistematik menunjukkan bahawa keadaan sintesis optimum untuk menghasilkan ZnO tanpa dop adalah dengan menggunakan 0.3 g serbuk Zn, 30 minit tempoh sintesis, dan 5 cm jarak substrat Si dari serbuk Zn pada 650 °C. Purata panjang, diameter, aspek nisbah dan ketumpatan areal masing-masing ialah 2.99 ± 0.13 μm, 0.54 ± 0.05 μm and 5.6 ± 0.3, 2.9 ± 0.9 rods/μm^2. Kemudian, cara Fe-dop *ex-situ* telah dijalankan melalui semburan pirolisis ke atas rod ZnO tanpa dop. Ciri-ciri fizikal Fe-dop rod ZnO yang telah dihasilkan melalui pendopan *ex-situ* akan dibandingkan dengan Fe-dop rod ZnO yang telah dihasilkan melalui pendopan *in-situ* pada fasa yang berikutnya. Kehadiran puncak Fe $2p_{1/2}$ dan Fe $2p_{3/2}$ pada 722.3 eV dan 705.7 eV masing-masing dalam analisis Spektroskopi X-Ray (XPS) mendedahkan penggantian Fe^{2+} dengan Zn^{2+} dalam rod ZnO tanpa dop.

Berbanding dengan rod ZnO tanpa dop, Fe-dop rod ZnO menunjukkan pengurangan fotodegradasi RhB di bawah sinaran cahaya ultraungu (UV). Akhir sekali, pendopan Fe melalui cara *in-situ* telah berjaya dihasilkan untuk mensistesis Fe-dop rod ZnO dengan menggunakan AA-CVD. Fe-dop rod ZnO telah disintesis pada keadaan 0.05 M bahan dop Fe, 60 minit tempoh pendopan dan 650 °C. Purata panjang dan diameter masing-masing adalah 4.45 ± 0.26 µm dan 0.71 ± 0.05 µm. Puncak Fe $2p_{1/2}$ dan Fe $2p_{3/2}$ pada 718.4 eV dan 704.8 eV masing-masing hadir dalam keadaan Fe^{3+}. Berbanding dengan pendopan *ex-situ*, Fe-dop rod ZnO yang disintesis oleh cara pendopan *in-situ* menunjukkan ciri-ciri yang serupa, iaitu (i) peralihan puncak (002) Diffraktometer X-Ray (XRD) kepada nilai yang lebih kecil; (ii) penurunan nisbah I_{uv}/I_{vis} bagi Fotoluminesen (PL) pada suhu pengukuran bilik; dan (iii) pengurangan aktiviti fotodegradasi. Walaupun pendopan *ex-situ* dan *in-situ* berolehkan Fe^{2+} dan Fe^{3+}, kedua-dua teknik tetap sama menunjukkan pengurangan aktiviti fotodegradasi. Dengan pengurangan aktiviti fotokatalitik dan kebolehan penyerapan UV yang baik, Fe-dop ZnO rod boleh menjadi calon yang berpotensi sebagai pelindung UV.

SYNTHESIS AND CHARACTERIZATION OF Fe-DOPED ZINC OXIDE RODS

ABSTRACT

Chemical Vapor Deposition (CVD) technique is the most common vapor route technique uses by researchers to synthesize ZnO nanostructures. However, the current *in-situ* doping approaches using CVD do not give many flexibilities for the researchers to produce doped ZnO nanostructures. As the dopant solution is kept outside the furnace, the Aerosol Assisted - Chemical Vapor Depostion (AA-CVD) is a potential *in-situ* doping technique because it offers many advantages such as flexibility of controlling the doping concentration, doping duration, type of dopant precursor and possibility of mass production of doped nanostructures. This project started by setting up a CVD system to synthesize undoped ZnO rods without using foreign catalyst. The study indicated that the optimum synthesis condition for synthesizing undoped ZnO rods was using 0.3 g Zn powder, 30 min synthesis duration, and 5 cm distance of Si substrates from Zn powder at 650 °C. The average length, diameter, aspect ratio and areal density of undoped ZnO rods are 2.99 ± 0.13 μm, 0.54 ± 0.05 μm, and 5.6 ± 0.3, 2.9 ± 0.9 rods/μm^2, respectively. Subsequently, *ex-situ* Fe-doping was performed via spray pyrolysis on the pre-grown ZnO rods. The physical properties of Fe-doped ZnO rods prepared by *ex-situ* doping would be used to compare with the Fe-doped ZnO rods prepared by *in-situ* doping in the subsequent phase. The presence of Fe $2p_{1/2}$ and Fe $2p_{3/2}$ peaks which were located at 722.3 eV and 705.7 eV, respectively in (X-Ray Spectroscopy) XPS analysis reveals the substitution of Fe^{2+} with Zn^{2+} in the ZnO rods. As compared to undoped ZnO rods, the Fe-doped ZnO rods exhibited poor photocatalytic activity in degradation of

RhB dye under UV irradiation. Lastly, *in-situ* Fe-doping was successfully performed to synthesize Fe-doped ZnO rods using AA-CVD. At the synthesis condition of 0.05 M dopant solution, doping duration of 60 min and 650 $^{\circ}$C, Fe-doped ZnO rods were synthesized. The average length and diameter were 4.45 ± 0.26 µm and 0.71 ± 0.05 µm, respectively. The Fe $2p_{1/2}$ and Fe $2p_{3/2}$ peaks of XPS which located at 718.4 eV and 704.8 eV, respectively present in the form of Fe^{3+} state. As compared to *ex-situ* doping, the Fe-doped ZnO rods synthesized by *in-situ* doping demonstrated similar properties, i.e., (i) the shift of (002) X-Ray Diffraction (XRD) peak to a smaller 2θ; (ii) the reduction of I_{uv}/I_{vis} ratio of room temperature Photoluminescence (PL) measurement and; (iii) poor photodegradation activity. Although Fe^{2+}, and Fe^{3+} state were obtained for both *ex-situ* and *in-situ* doping respectively, both techniques similarly showed poor photodegradation activity. The Fe-doped ZnO rods with poor photocatalytic activity but good UV absorption capability could be a potential UV shielding candidate.

CHAPTER 1
INTRODUCTION

1.1. Introduction

Zinc oxide (ZnO) is one of the important semiconductor materials due to its direct wide bandgap of 3.37 eV and a large exciton binding energy (60 meV) at room temperature. These unique properties ensure efficient exciton emissions at room temperature. Thus, it is a potential candidates for numerous applications such as light emitting diodes (LED) (Wang *et al.*, 2009), transparent electrodes (Goris *et al.*, 2008), photocatalysts (Mills *et al.*, 2007), sensitized solar cells (Law *et al.*, 2005), and flat panel displays (Lee *et al.*, 1997). In addition, ZnO has a stable wurtzite crystal structure without a centre of symmetry. This results in strong piezoelectric and pyroelectric properties along its [0001], which are suitable for the fabrication of mechanical actuators and piezoelectric sensors (Wang, 2004b).

The early research of ZnO could be back tracked as early as 1930s (Heiland et al., 1959, Brown, 1976, James and Johnson, 1939) and the research peaked around the end of 1970s (Klingshirn, 2007). In this period of time, extensive works had been done on ZnO bulk samples, covering topics such as growth techniques, doping, and optical properties of ZnO. Presently, the emphasis of ZnO researches are on nanostructures, particularly the synthesis and doping techniques as well as ZnO nanostructures based applications.

Various approaches have been developed for growing ZnO nanostructures. These approaches generally can be divided into two routes, i.e. the vapor route and solution route. The most common vapor route to synthesize ZnO nanostructure is

chemical vapor deposition (CVD) technique (Fan and Lu, 2006, Meng et al., 2010, Chang et al., 2004, Grabowska et al., 2005, Wang et al., 2004, Wu and Liu, 2002, Li *et al.*, 2003). Other vapor route techniques include physical vapor deposition (PVD) (Feng et al., 2010) and atomic layer deposition (ALD) (Pung *et al*., 2008) have been used to synthesize ZnO nanostructures. The vapor route techniques normally produce high crystal quality ZnO nanostructures attribute to its high synthesis temperature and/or high purity precursors. These high crystal quality ZnO nanostructures are suitable for the application in opto-electronic (Wang *et al.*, 2009). However, these techniques operate at high synthesis temperature; incur high equipment cost and/or operational costs. For example, temperature as high as 1380 °C was needed to vaporize ZnO powder for the growth of ZnO rods via CVD technique (Fan and Lu, 2006). In addition, a small R&D unit of ALD system could easily costs USD 250,000 (Pung *et al*., 2008).

In solution routes, methods such as sol-gel (Ahn et al., 2004), hydrothermal (Tam et al., 2006) and electrodeposition (Jiang Feng et al., 2010) have been widely used to synthesize ZnO nanostructures. Advantages of using solution route to synthesize nanostructures are their low synthesis temperature (normally < 100^{o}C), low equipment cost and possibility of producing ZnO nanostructures in large scale. However, the ZnO nanostructures synthesized via solution route have relatively poor crystal quality attributed to its low synthesis temperature and precursors. The nanostructures contain high concentration of impurity and crystal defects (Glushenkov and Chen, 2006).

ZnO is naturally *n*-type semiconductor due to the present of point defects such as oxygen vacancies (V_o), zinc interstitials (Zn_i)) and hydrogen in its crystal lattice (Yogamalar and Bose, 2013). Therefore, doping in ZnO with selective elements offers great potential to adjust their electrical, optical and magnetic properties. Since ZnO is a compound semiconductor, substitution of Zn or O with other atoms can be possibly done to produce *n*-type ZnO. It is found that substitutions of Zn with group III elements are commonly reported by researchers to produce *n*-type ZnO. For instances, Al (Agura et al., 2003), Ga (Yuan et al., 2008) and, In (Jung et al., 2009) were used as dopants to produce *n*-type ZnO nanostructures. The other possibility for n-doping would be to use Group VII elements such as F (Pawar et al., 2008), and Cl (Chikoidze et al., 2008) to substitute O. This approach is rarely reported in literature.

The *p*-type ZnO could be produced using group- I elements, such as Li (Zeng et al., 2006), Na (Lin et al., 2008) and K (Xu et al., 2008), to substitute into Zn sites. Also, it can be achieved by substituting group-V elements, such as N (Lu et al., 2007), P (Hsu et al., 2005) and As (Ryu et al., 2000), into O sites. Lately, the co-doping approach, i.e, by using either two different acceptors simultaneously (e.g. ZnO : N, P) (Tian and Zhao, 2009) or by combining a moderate concentration of donors with a higher concentration of acceptors (e.g. in ZnO:Ga,N) (Joseph et al., 1999) successfully produced *p*-type ZnO. Despite tremendous effort have been done by researchers, it is difficult to produce a stable *p*-type ZnO. This is because the defects such as oxygen vacancies (V_o), zinc interstitials (Zn_i) and hydrogen, which act as donors, hinder the formation of *p*-type ZnO. Moreover, some of these dopants

form deep level acceptors (Park et al., 2002) and thus are not likely useful to produce *p*-type ZnO.

It is crucial to control the concentration of dopants in order to tailor the physical properties of ZnO nanostructures. Many doping techniques have been developed, which can generally be classified into *ex-situ* doping and *in-situ* doping. In *ex-situ* doping, the dopants are normally diffused into the pre-grown ZnO nanostructures via post-annealing. For examples, Piticescu et al. synthesized Al-doped ZnO nanopowders by two step of hydrothermal and evaporation condensation technique (Piticescu et al., 2006). Lee and Park synthesized Al-doped ZnO thin film by spray pyrolysis and post-annealing technique (Lee and Park, 2004). This approach produced Al-doped ZnO nanopowder with good crystal quality and a smaller grain size. In *in-sit*u doping, the dopants will be incorporated into the lattice structure of ZnO during the synthesis process. For instances, Liu et al. synthesized In-doped ZnO NWs using mixture of ZnO, In_2O_3 and graphite powder at 935 °C for 40 min. In-doping in ZnO NWs induced many oxygen vacancies and exhibit intrinsic ferromagnetism at room temperature (Liu et al., 2010). Jung et al. grew Sn-doped ZnO NWs using mixture of ZnO-graphite powder, and SnO powder at 1050 °C (Jung et al., 2011). On the other hand, Sn doping enhanced the green emission intensity of ZnO NWs as a result increases of the number of oxygen vacancies in the crystal lattice. This was proven by XPS compositional analysis. Bin et al. synthesized Fe-doped ZnO nanocantilevers by vapor phase process using amorphous Zn-Fe-C-O composite powder at 900 °C (Bin et al., 2008). The XPS and Raman spectrum confirmed substitution of the Fe^{3+} into the ZnO lattice at Zn^{2+} site. Red shift of the

UV emission band of Fe-doped ZnO nanocantilevers was observed in PL measurement.

1.2. Problem Statement

Although extensive studies have been done on ZnO nanostructures, there is still much science that needs to be explored and improved for a better engineering of their properties. The two main problems to be addresses in this project are:

(i) Lacking of an effective *in-situ* doping technique via CVD process to synthesized doped ZnO nanostructures.

The common in doping approach via CVD process was done by mixing both the dopant precursor and Zn related precursors together (Liu et al., 2010, Jung et al., 2011, and Mohan et al., 2012). The limitation of mixing both the dopant sources together with the Zn related precursor is that the dopant source must have a close evaporation/sublimation temperature with the Zn related precursor. This criterion is important to ensure a sufficient amount of dopant vapor is generated during the synthesis of nanostructures for *in-situ* doping purpose. In fact, Wang et al., reported that synthesis of Al-doped ZnO NWs was difficult by mixing the Al powder with the Zn precursor via CVD technique. This is because the Al vapor pressure is much lower than Zn by an order of 10^{-12} at 550 ^{o}C (Wang et al., 2006). Also, various issues such as undesired transformation of rods into nanobelts (Jie et al., 2004, Hong Jin et al., 2006), formation of In_2O_3 secondary phase (Jie *et al*., 2004) and hierarchical structures (Liu and Zeng, 2004) were encountered.

In order to rectify the above problem, the dopant precursor and Zn related precursor were placed separately at different heating zone in the reactor (Hong Jin et

al., 2006). Although the doping efficiency might be able to improve via this arrangement, the above approach is limited to laboratory scale for producing doped nanostructures. Furthermore, it is difficult in controlling the doping concentration and duration, as well as lack of flexibility in choosing the suitable dopant precursor. Synthesis techniques such as Molecular Beam Epitaxy (MBE) and Metal Organic Chemical Vapor Deposition (MO-CVD) have great potential for mass production of doped nanostructures. However, these techniques incur high equipment and processing cost. The above limitations in existing *in-situ* doping by CVD technique could be rectified by AA-CVD.

(ii) Limited application of ZnO as UV shielding agent attributed to its inherent photocatalytic activity.

Another issue related to ZnO is of its application as UV shielding agent. It is well known that long exposure of UV light causes degradation of polymeric materials and organic dyes. Therefore, the development of effective UV shielding agents using wide bandgap semiconductor materials such as ZnO is of great importance. In fact, ZnO has been regarded as UV absorber/filter in outdoor textiles, sun blocks, car window, and practical UV shielding applications (Barker and Branch, 2008, Becheri et al., 2008). However, further development of ZnO-based UV absorber/filter was hindered due to the inherent photocatalytic activity of ZnO. The absorbed UV rays will generate electron-hole pairs when the irradiation energy exceeds bandgap energy of ZnO. The photo-generated electron-hole pairs cause oxidation reactions occur on the surface of ZnO, forming reactive free radicals such as superoxide (O^{2-}) and hydroxyl ($^{\bullet}OH$) which in turn causes photocatalysis. This results in the fading of fabric, deterioration of paints, and skin damage (Sun et al.,

2009). Hence, in order to utilize ZnO as UV protection applications, it is crucial to effectively reduce the photocatalytic activity of ZnO while maintaining its capability to absorb UV light.

The potential of aerosol-assisted chemical vapor deposition (AA-CVD) technique to produce doped ZnO rods via *in-situ* doping was explored in this project. As the dopant solution is kept outside the furnace, it offers many advantages such as a wider choice of dopant precursors as long as the dopant precursor can be dissolved in water and/or organic solvent such as methanol. Thus, consideration of matching the partial pressure of dopant precursor and Zn related precursor during the synthesis for effective doping is not critical. The solution of dopant precursor can be refilled when necessary during the synthesis process. In addition, this technique offers the ease of controlling the dopant concentration and doping duration. The timing to supply the dopant aerosol into the reactor is flexible. Thus, the dopant aerosol can be supplied to the reactor only when the reactor reaches the required synthesis temperature and pressure for the growth of nanostructures. Besides, AA-CVD incurs low equipment and operation costs. It can be operated under low pressure or atmospheric pressure synthesis environment. Therefore, AA-CVD can be adapted easily for mass production of doped semiconductor nanostructures. Briefly, AA-CVD avoids the major constraints of conventional CVD approach for *in-situ* doping.

ZnO nanostructures doped with transition metal (TM) such as Fe, Co, Ni, Cu, Cd and Mn have been widely studied for the spintronics and magnetic applications (Yogamalar and Bose, 2013). The 3d TM ions can be readily adopted in the Zn state. This helps in achieving higher TM dopant concentrations as they favors substitution

of the TM ion at the cation site (Rebecca et al., 2005). According to Hong *et al*. study, Fe dopant exhibited strong ferromagnetic saturation magnetization of 6.38 memu/g as compared to various TM dopants (Hong et al., 2011). However, the photocatalytic activity of these TM doped ZnO is rarely studied by researcher. Therefore, Fe was selected as dopants for ZnO rods in this project.

1.3. Research Objectives

i. To synthesize undoped ZnO rods using CVD technique,

ii. To synthesize Fe-doped ZnO rods using spray pyrolysis technique (*ex-situ* doping),

iii. To synthesize Fe-doped ZnO rods using AA-CVD technique (*in-situ* doping), and

iv. To study the photocatalytic activity of undoped ZnO rods and Fe-doped ZnO rods in degradation of RhB dyes under UV light.

1.4. Scope of study

A CVD system was setup to synthesize undoped ZnO rods using Zn powder and O gas as precursors. As Fe-doped ZnO rods would be studied in this project, the ZnO rods were synthesized by CVD without using foreign catalyst to avoid unintentional doping by the foreign catalyst. A systematic study was conducted by changing the synthesis parameters such as amount of Zn powder, substrate location and synthesis duration in order to establish the optimum process window for the growth of ZnO rods in the subsequent phases.

Next, Fe-doped ZnO rods were produced using spray pyrolysis technique via *ex-situ* doping. Synthesis parameters such as concentration of dopant solution and doping duration were systematically studied. The Fe-doped ZnO rods prepared by *ex-situ* doping were used for comparison purpose as it was likely that the Fe dopants from the aerosol would be driven into the pre-grown ZnO rods at 650 ^{o}C. Thus, the structural, optical properties and photocatalytic activities of these Fe-doped ZnO rods would be used as references to compare with the Fe-doped ZnO rods synthesized via *in-situ* doping using AA-CVD.

Lastly, a novel *in-situ* doping technique, i.e. based on AA-CVD was established to produce Fe-doped ZnO rods. The physical properties and photocatalytic activity of these Fe-doped ZnO rods were compared with the undoped ZnO rods and the Fe-doped ZnO rods that prepared by *ex-situ* doping, i.e. spray pyrolysis technique.

In this work, Field Emission Scanning Electron Microscopy (FE-SEM) was used to characterize the surface morphology of the undoped and Fe-doped ZnO rods. X-Ray Diffraction (XRD) was used to identify the phase presence and the crystal structure. The elemental analysis was determined with Energy Dispersion X-Ray (EDX). Transmission Electron Microscope (TEM) was used to get information about the morphology, and crystallographic information of the Fe-doped ZnO rods. Meanwhile, high sensitive surface analysis of X-Ray Photoelectron Spectroscope (XPS) was used to identify the chemical stoichiometric of Fe-doped ZnO rods samples. Photoluminescence (PL) was used to characterize the optical properties of the ZnO rods and Fe-doped ZnO rods. Ultraviolet/Visible Spectroscope (UV-Vis)

was used to investigate the degradation efficiency of Rhodamine-B dye (RhB) solution by the photocatalytic activity of ZnO rods and Fe-doped ZnO rods under UV irradiation.

1.5. Outline of dissertation

This dissertation is organized into five chapters. In Chapter 1, the introduction of this research work, problem statement, research objectives, the scope of research as well as dissertation overview are presented. Chapter 2 comprises of literature review on the properties of ZnO, various synthesis techniques of ZnO nanostructures, doping of ZnO nanostructures and its applications. The specifications of the raw materials, research methodology and the characterization techniques employed in this research work are described in Chapter 3. The results and discussions on the synthesis of undoped ZnO rods and Fe-doped ZnO rods are presented in Chapter 4. Lastly, Chapter 5 summarizes the key findings of this project as well as several suggestions and recommendations for the future work.

CHAPTER 2
LITERATURE REVIEW

2.1. Zinc Oxide (ZnO)

ZnO has attracted research focus due to its unique properties, versatility and compatibility in numerous applications. The fundamental characteristics features of ZnO includes direct wide band gap (3.37 eV), large excitation binding energy (60 meV), near UV emission, transparent conductivity, piezoelectric property, bio-safe and bio-compatible.

Like most of other wide band gaps semiconductors, ZnO has been studied extensively in the early 70s. The research on ZnO was mainly emphasized on the ZnO bulk and thin films, covering topics such as synthesis methods, doping, structural, electrical and optical properties (Klingshirn, 2007). The current research of ZnO covers similar topics but more attention is given on the synthesis, characterization and application-related aspects of ZnO nanostructures (Klingshirn, 2007). As shown in Fig. 2.1, various ZnO nanostructures such as nanorods, nanowires, nanocombs, nanotubes, nanobelts, nanosprings, nanorings, nanobows and nanopropellers could be synthesized by adjusting the synthesis parameters or using different types of catalyst (Wang, 2004a).

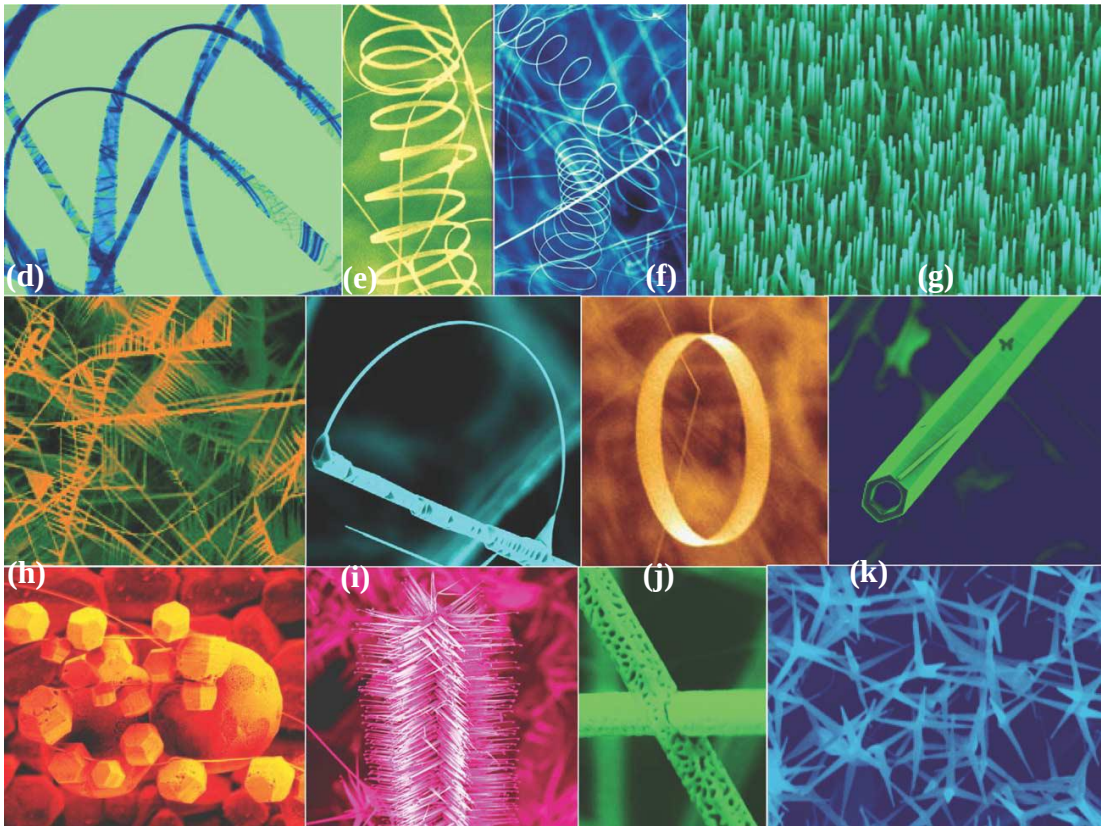

Fig. 2.1. Examples of ZnO nanostructures of (a) nanobelt, (b) nanohelixes, (c) nanorods, (d) nanocomb, (e) nanobows, (f) nanorings, (g) nanotubes, (h) nanocages, (i) nanopropellers, (j) high porosity nanowires, and (k) nanotetrapod that were synthesized under controlled conditions by thermal evaporation of solid powders (Wang, 2004a).

2.2. Properties of ZnO

2.2.1. Crystal structure

ZnO is one of the II-VI binary compound semiconductors. Generally, it can presence in Rocksalts, Zinc blend or Wurtzite crystal structures as illustrated in Fig. 2.2. The Rocksalts or Rochelle salt (NaCl) crystal structure is obtained at relatively high pressure (Fig. 2.2 (a)) (Özgür, 2008) whereas Zinc blende crystal structure (Fig.

2.2 (b)) is stable only by epitaxial growth of ZnO on cubic substrates (Klingshirn, 2007). The ZnO is commonly found in wurtzite structure (Fig. 2.2 (c)) with lattice parameters of a = 0.3296 nm and c = 0.5207 nm as it is thermodynamically stable at ambient temperature. The tetrahedrally ZnO composes of zinc (Zn) ions and oxygen (O) ions, where each of the Zn ion is surrounded by four O ions, and vice versa. The Zn ions and O ions are stacked alternately along the c-axis (Wang, 2004b). Consequently, the polarity of ZnO is developed along its c-axis, making ZnO inherent with excellent piezoelectric property (Shulin and Changhui, 2009). The polar surfaces of ZnO are (±0001) with superior stability. They are atomically flat and stable. The other two commonly observed facets of ZnO are non-polar surfaces of $\{2\bar{1}\bar{1}0\}$ and $\{01\bar{1}0\}$. These two planes have a lower energy compare to {0001} facets.

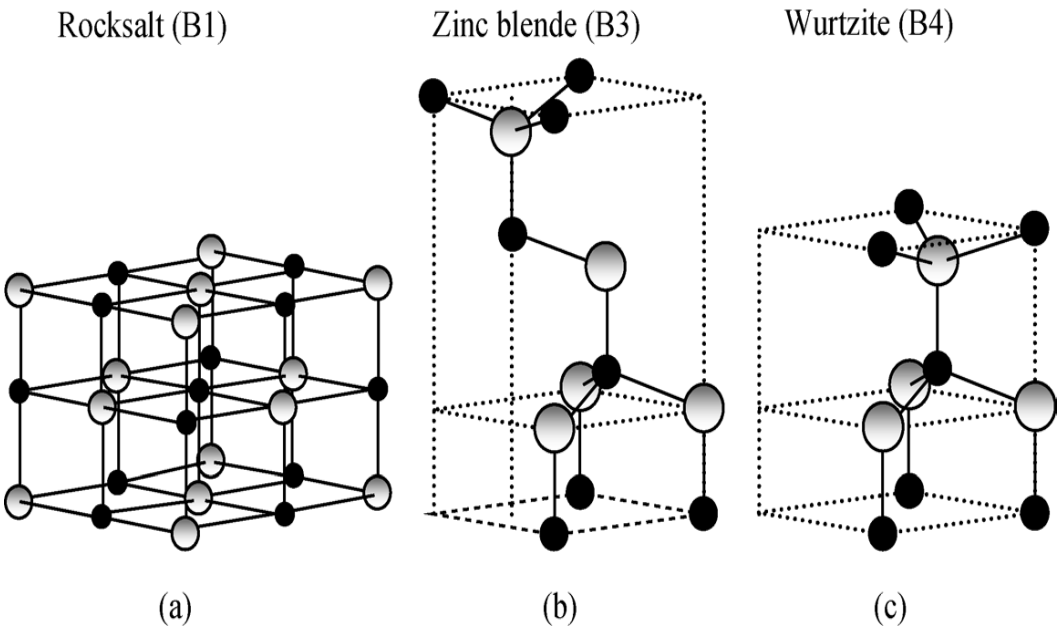

Fig. 2.2. ZnO crystal structures of (a) cubic rock salt, (b) cubic zinc blende, and (c) hexagonal wurtzite. The shaded gray and black spheres denote Zn atoms and O atoms, respectively (Özgür, 2008).

2.2.2. Optical property

ZnO is known as a promising photonic material for the light emission in the blue-UV region because of its direct band gap of 3.37 eV. The large exciton energy (60 meV) at room temperature of ZnO ensures an efficient exciton emission under low excitation energy. The optical properties of ZnO are commonly studied by photoluminescence (PL) spectroscopy at room temperature (RTPL). As shown in Fig. 2.3, a typical ZnO PL spectra consists of a sharp UV emission (~378 nm, Near Band Edge emission, NBE) and possibly one or more visible bands (450-700 nm) (Djurišić and Leung, 2006, Kuo and Lin, 2014). The strong UV emission is attributed to the free excitons recombination from a near band-edge (NBE) transition of wide band gap of ZnO (Wang et al., 2009a).

In contrary, the deep level visible emission happened due to the presence of various defects (recombination centers) in ZnO (Djurišić and Leung, 2006, Rui Zhang 2009). Thus, the ratio of I_{UV}/I_{Vis} of RTPL spectra indirectly indicates the crystal quality of the ZnO (Wang et al., 2003b).

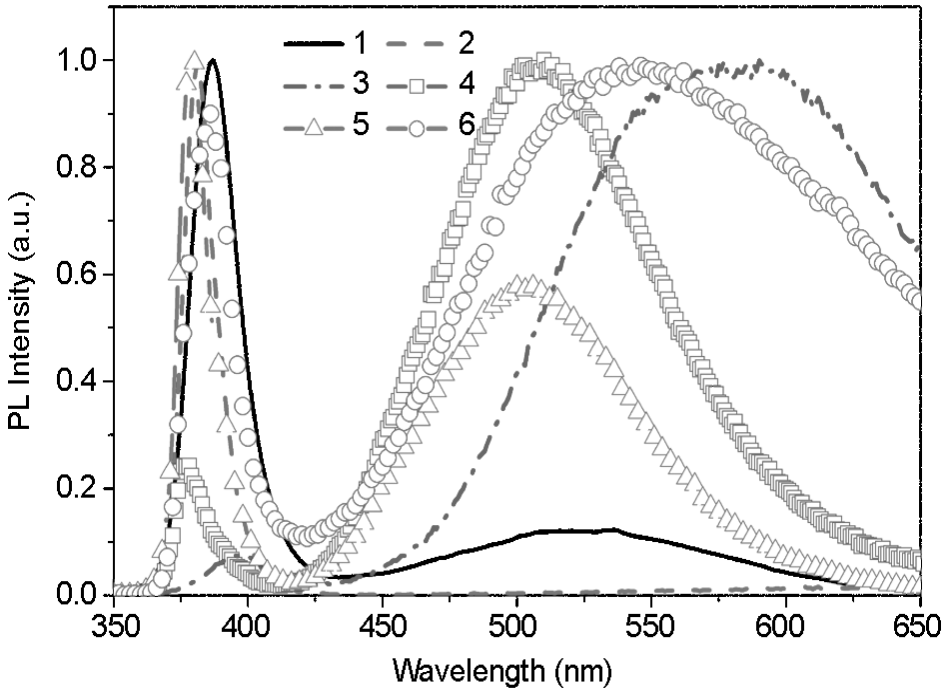

Fig. 2.3. Room-temperature PL spectra of ZnO nanostructures: (1) tetrapods, (2) needles, (3) nanorods, (4) shells, (5) highly faceted rods, (6) ribbons/combs (Djurišić and Leung, 2006).

2.2.3. Electrical property

ZnO is a *n*-type semiconductor material in nature due to the formation of native defects such as O vacancies and Zn interstitials (Yogamalar and Bose, 2013). Thus, the majority charge carriers of ZnO are electrons. It is reported that the electron mobility of ZnO thin film under electrical field could achieved as high as 7 cm^2/Vs (Fan and Lu, 2005). However, the single crystal ZnO NW synthesized by CVD demonstrated superior electrical properties as compared to the ZnO thin films. The reported electron mobility of undoped ZnO NW was 80 cm^2/Vs, which was about 11 times larger than the ZnO thin films (Chang et al., 2004). The doped n- and *p*-type ZnO NWs typically have the electron mobility of 200 and 5-50 cm^2/Vs, respectively at room temperature as the consequence of the charge carrier scattering

(Özgür et al., 2005). The electron mobility of ZnO NW could be further improved to 1000 cm^2/Vs by coating the NW with polyimide in order to reduce the electron scattering and trapping at the surface of ZnO NW (Park et al., 2004b). The hole mobility of ZnO is much lower than the electron mobility due to the difference of effective mass and carrier scattering mechanism (Choi et al., 2010). Typical hole mobility of ZnO thin films/NWs falls in the range 5 to 50 cm^2/Vs (Norton et al., 2004).

Another important electrical parameter of ZnO is charge carrier concentration. The undoped ZnO NWs have charge carrier concentration of 1.7×10^7 cm^{-3} (Fan et al., 2004). A higher carrier concentration of $\sim10^{20}$ electrons.cm^{-3} and $\sim10^{19}$ holes.cm^{-3} could be achieved by surface modification through *n*-type and *p*-type doping respectively (Choi et al., 2010). Fig. 2.4 shows the TEM images and I-V curves of the undoped and In-doped ZnO NWs having the charge carrier concentration of 1.2×10^{17} cm^{-3} and 4.8×10^{17} cm^{-3} respectively. In-doped ZnO NWs shows increase in the conductivity as the result of increase in the mobility. It introduces changes in electrical and optical properties which the band gap was altered. The band gap widen is usually assigned to variations in carriers concentrations and formation of an impurity band near the band edge of the conduction band. The calculation of the doping of ZnO NWs with In enhanced the conductivity by a factor of 14 (Ahmad and Zhu, 2011).

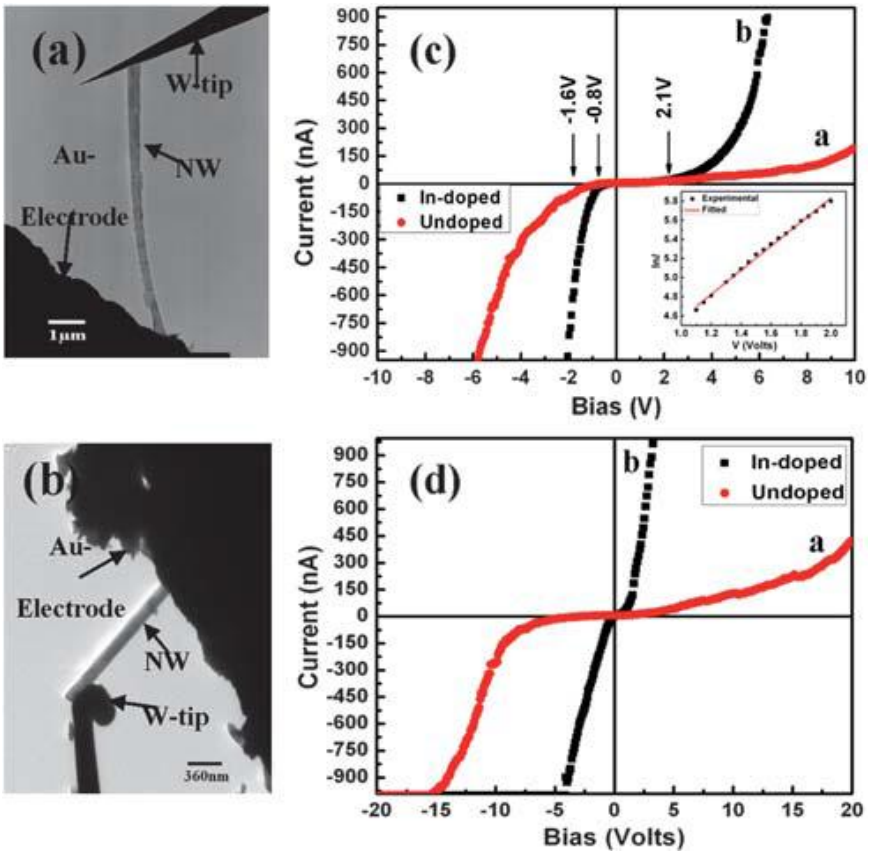

Fig. 2.4. TEM images of (a) In-doped and (b) undoped ZnO NWs used for *in-situ* current–voltage (I–V) measurements. (c) Corresponding I–V curves for the undoped and In-doped ZnO NWs. (d) I–V curves for the undoped and In-doped ZnO NWs at high bias (Ahmad et al., 2009).

2.2.4. Piezoelectric property

As illustrated in Fig. 2.5, wurtzite ZnO is lacking of a centre of symmetry in its crystal structure. The Zn^{2+} cations are surrounded tetrahedrally by O^{2-} anions in which the center of gravity of the O atoms is at the center of tetrahedron. As the consequence of the external pressure applied on the crystal, the distortion of Zn^{2+} cations and O^{2-} anions happen thus generating electric dipole. The piezoelectric effect converts a mechanical vibration into an electrical signal or vice versa. This property has been utilized in the applications of resonators, micro-dispensing system,

sensors for vibration waves in air and under sea and, controlling tip movement in scanning probe microscopy.

ZnO structures have a strong piezoelectric and pyroelectric property. This enables ZnO in the form of NWs and nanobelts to be used as mechanical actuators and piezoelectric sensors as reported by (Wang, 2004b).

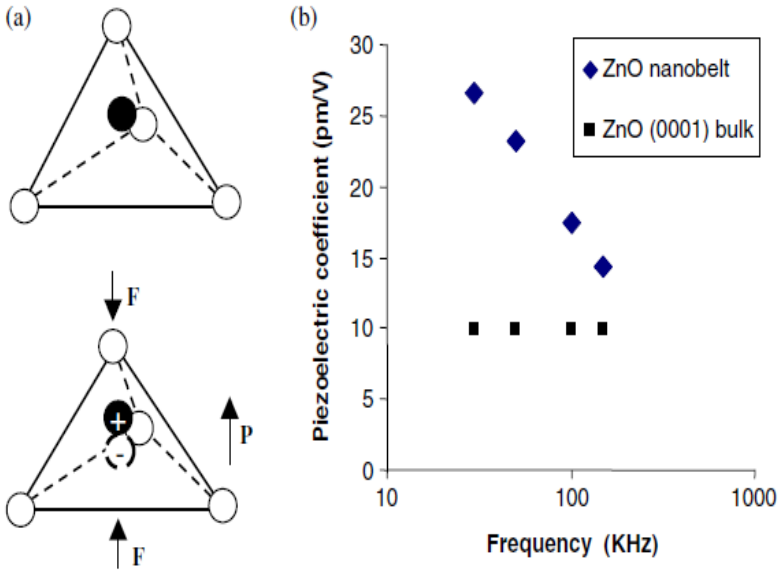

Fig. 2.5. (a) Schematic diagram illustrates the piezoelectric effect in a tetrahedrally coordinated cation-anion unit of ZnO crystal and (b) Piezoelectric coefficient (d_{33}) of ZnO bulk and ZnO nanobelts (Wang, 2004b).

2.3. Synthesis of ZnO nanostructures

2.3.1. Vapor route versus solution route

Many synthesis techniques have been developed to produce ZnO nanostructures. These techniques can be divided mainly into vapor route and solution route. The most common vapor route to synthesize ZnO nanostructure is chemical

vapor deposition (CVD) technique (Fan and Lu, 2006, Meng et al., 2010, Chang et al., 2004, Grabowska et al., 2005, Wang et al., 2004, Wu and Liu, 2002, Li *et al.*, 2003). Generally, vapor route produces ZnO nanostructures with a better crystal quality although the equipment setup could be costly. Examples of vapor route synthesis techniques are low pressure chemical vapor deposition (LP-CVD) (Wu and Liu, 2002), atmospheric pressure chemical vapor deposition method (AP-CVD) (Wang et al., 2003b), carbothermal reduction method (Meng et al., 2010), metal organic – chemical vapor deposition (MO-CVD) (Jeong et al., 2004) and physical vapor deposition (PVD)/thermal evaporation (Feng et al., 2010). Table 2.1 lists some of the common vapor route synthesis techniques used for the growth of ZnO nanostructures by researchers.

Schematic representation of a LP-CVD system for the growth of ZnO nanostructures is shown in Fig. 2.6 (Sood et al., 2007). The synthesis system consisted of a horizontal tube furnace, a vacuum pump and a gas supply system. The Zn precursor was located in the middle of the furnace (heating zone) and the substrates were located at the down stream of the furnace. The vaporized Zn precursor was transported to down stream, reacting with O_2 gas for the growth of ZnO nanostructures. There are several synthesis parameters to be controlled in order to produce ZnO nanostructures with desired morphology and geometry. This includes temperature (Dalal et al., 2006), type of substrates (Wu and Liu, 2002), carrier gas flow rate (Wang, 2004b), pressure (Dalal et al., 2006), and period of evaporation (Grabowska et al., 2005). A details discussion of the effects of synthesis parameters on the growth of ZnO nanostructures using vapor route techniques will be presented in section 2.3.3.

Table 2.1.Synthesis of ZnO nanostructures via vapor route.

Method	**Precursors/ substrate**	**Synthesis conditions/ Type of ZnO nanostructures**	**References**
AP-CVD	ZnS (99.99%), O_2 from atmosphere / Si substrate	1200°C for 180 min, Ar as carrier gas / NWs	(Wang et al., 2004a)
LP-CVD	Zinc acetylacetone hydrate ($Zn(C_5H_7)_2)_2.xH_2O$) (98%), O_2 gas / fused silica, Si (100), and sapphire (110) substrates	130-140°C, N_2 as carrier gas, 200 Torr / NRs	(Wu and Liu, 2002)
Carbothermal reduction CVD method	Mixture of ZnO powder and graphite powder / Si substrate	900°C for 30 min, Ar as carrier gas / NWs	(Meng et al., 2010)
Carbothermal reduction CVD method	Mixture of ZnO powder and graphite powder / Si, and Al_2O_3 substrate	950-1125°C for 30 min, Ar as carrier gas, Au catalyst/ NRs/NWs	(Grabowska et al., 2005)
Thermal evaporation	Zn source (99.99%), O_2 /Si substrates with pre-deposited ZnO film by PLD.	800°C for 30 min, N_2 as carrier gas (200 sccm) / NRs	(Feng et al., 2010)
RF magnetron sputtering	ZnO target / Sapphire substrate.	Power supply : 13.56 MHz, mean ion current density to the target: 1 $mAcm^{-2}$/ films	(Hwang et al., 2007)
MO-CVD	Diethyl zinc (DEZn) and high purity O_2 (2.45×10^{-3} and 1.21×10^{-2}) / Sapphire substrate.	360 and 500 °C, Ar as carrier gas / NWs and films	(Jeong et al., 2004)

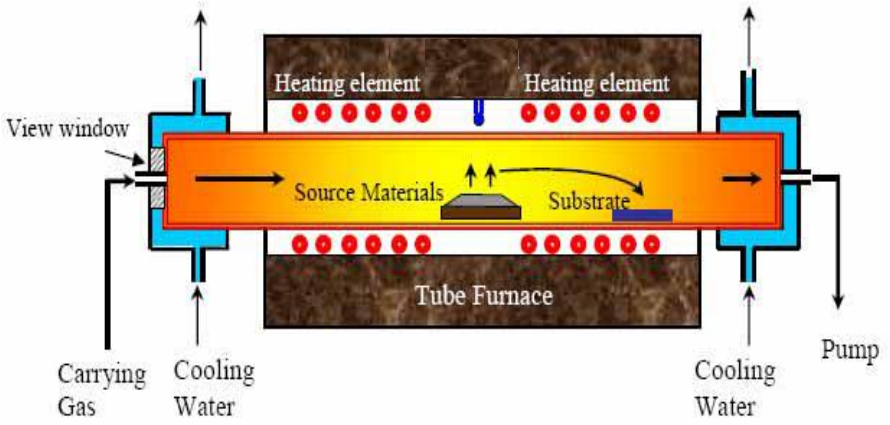

Fig. 2.6. A schematic diagram of LP-CVD system for the growth of ZnO nanostructures (Sood et al., 2007).

Synthesis of ZnO nanostructures via solution routes offer advantages such as low synthesis temperature (<100 °C), mass production capability, low equipment and operating cost. However, the ZnO nanostructures normally have relatively poor crystal quality attributed to its low synthesis temperature. The nanostructures contain high concentration of impurity and crystal defects (Glushenkov and Chen, 2006). Synthesis techniques such as hydrothermal (Tam et al., 2006), sol-gel (Ahn et al., 2004) and electro-deposition (Izaki et al., 2003) are frequently used by researchers for synthesis of ZnO nanostructures. The synthesis condition of various solution route techniques is summarized in Table 2.2. Fig. 2.7 shows the schematic flow of patterned ZnO NWs grown by hydrothermal method. The ZnO nanoparticle seed patterned was prepared from an aqueous solution containing zinc nitrate hydrate and HMTA in water. Solution routes synthesis techniques mostly requires additional steps such as annealing process in order to improve the crystal quality of ZnO nanoparticles. Fig. 2.8 shows the TEM image of ZnO NRs grown by hydrothermal method subjected to annealing process due to the poor crystal quality. However,

annealing in the reducing environment (forming gas) could caused surface damage and thinning of the rods (Tam et al., 2006).

Table 2.2. Synthesis of ZnO nanostructures via solution routes.

Method	Precursors/ substrate	Synthesis conditions	References
Hydrothermal	Sodium hydroxide and deionized water/ Zn foil	180 °C for 24 hours	(Tam et al., 2006)
Sol-gel	Zinc nitrate hexahydrate and methenamine solution / SiO_2 layer on Si substrate	95 °C for 1 /or 2 hours	(Ahn et al., 2004)
Sol-gel	Zinc nitrate hexahydrate and methenamine / polycrystalline F-SnO_2 glass, single crystalline sapphire, Si/SiO_2 wafers, or nanostructured ZnO thin film	95 °C for several hours.	(Vayssieres, 2003)
Template assisted – Sol gel	Zinc acetate suspension immersed together with AAM template	Immersion of 1 min continued by heating in air at 120 °C for 6 hours to obtain ZnO nanofibers.	(Lakshmi et al., 1997)

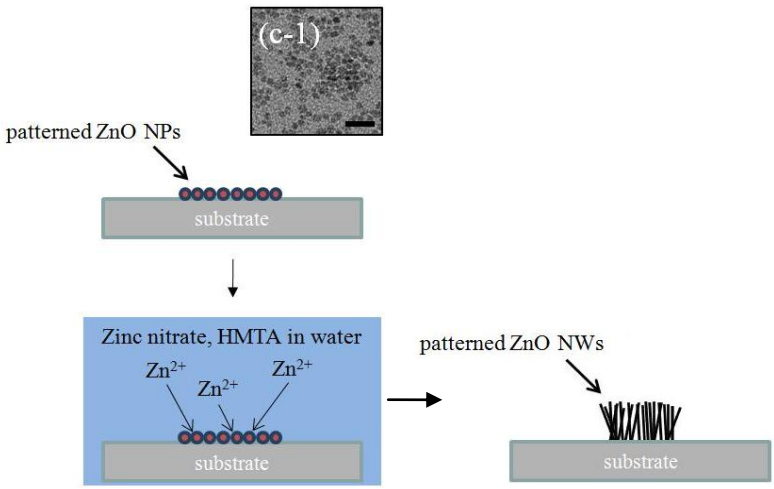

Fig. 2.7. A schematic flow of typical patterned ZnO NWs grown by hydrothermal method. (C-1) is the TEM image of ZnO NP seeds (scale bar = 15 nm).

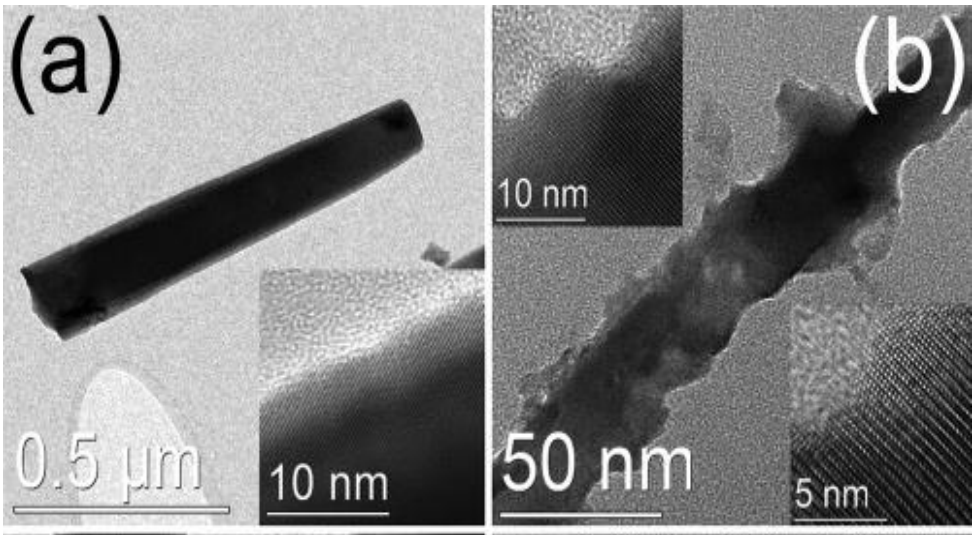

Fig. 2.8. Representative TEM images of ZnO nanorods: (a) as-grown, (b) annealed in forming gas at 600 °C. The insets show corresponding HRTEM images (Tam et al., 2006).

2.3.2. Effects of synthesis parameters on the growth of ZnO NRs via vapor route

2.3.2.1. Substrate distance from Zn source

The growth of ZnO NWs requires both the Zn vapor and O vapor. Thus, the amount of Zn/O vapor will determine the size of ZnO NWs. When the Zn powder vaporized, the Zn vapor concentration varied along the tube. Since the O_2 flow rate was kept constant throughout the process, thus the reduction in the length and diameter of ZnO NWs was due to the lack of Zn vapor. Fig. 2.9 shows the relationship between the length of the ZnO NWs and the deposition position. The longest NWs arrays were obtained in the up stream 6 cm away from the source, and the length reduced in the down stream due to the exhaustion of Zn vapor. The length at the distance of 6 cm, 10 cm, 15 cm and 18 cm are 99.3 ± 1.7 μm, 50.0 ± 0.5 μm, 12.6 ± 0.3 μm, and 1.1 ± 0.2 μm, respectively. The length of the ZnO NWs arrays to

nearly 100 μm could be achieved by adjusting proper deposition distance (Meng et al., 2010).

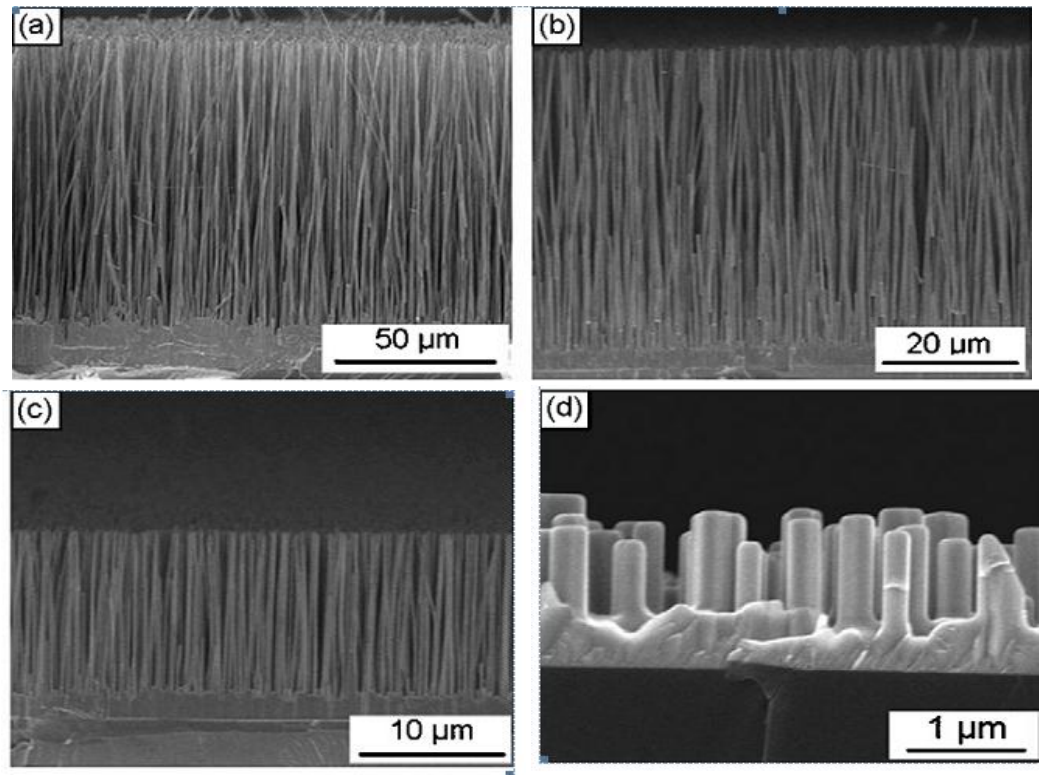

Fig. 2.9. FE-SEM cross section views of ZnO nanowire arrays obtained in pure O_2 carrier gas under a flow rate of 5 sccm O_2: (a)–(d) are nanowire arrays deposited at 6, 10, 15 and 18 cm away from the source. (Meng et al., 2010).

2.3.2.2. O and Zn vapor rich environment

Meng et al. (2010) studied the growth of ZnO NWs under O rich and Zn vapor rich environment using a quartz tube with only one opening as illustrated in Fig. 2.10 (a) (Meng et al., 2010). The Zn powder was kept at the sealed end, creating a Zn rich environment ($Zn_{(g)}$). In contrary, 5 sccm O_2 gas was flowed into the quartz tube at the open end, generating O rich environment ($O_{2(g)}$). The Zn vapors were transported to the open end due to concentration gradient and vice versa. The growth